Gondwana Research 95 (2021) 1–9

Contents lists available at ScienceDirect

Gondwana Research

journal homepage: www.elsevier.com/locate/gr

Different metal sources in the evolution of an epithermal ore system: Evidence from mercury isotopes associated with the Erdaokan epithermal Ag-Pb-Zn deposit, NE China

Changzhou Deng [a], Chenglu Li [b], Yimeng Rong [a], Di Chen [a], Ting Zhou [a], Xueyun Wang [a], Huayong Chen [c], Bernd Lehmann [d], Runsheng Yin [a,*]

[a] State Key Laboratory of Ore Deposit Geochemistry, Institute of Geochemistry, Chinese Academy of Sciences, Guiyang 550081, China
[b] Heilongjiang Institute of Natural Resources Survey, Harbin 150036, China
[c] Key Laboratory of Mineralogy and Metallogeny, Chinese Academy of Sciences, Guangzhou 510640, China
[d] Mineral Resources, Technical University of Clausthal, Clausthal-Zellerfeld 38678, Germany

ARTICLE INFO

Article history:
Received 18 December 2020
Revised 7 March 2021
Accepted 18 March 2021
Available online 29 March 2021

Keywords:
Subduction zones
Epithermal deposit
Hg isotope
Mass independent fractionation
Metal source

ABSTRACT

Epithermal metal deposits along convergent plate margins are of large economic value, however, the origin of the typical metal spectrum (Au, Ag, Sb, As, Hg) in these deposits remains debated. Here, we study the Hg isotope geochemistry of the vein-style Erdaokan Ag-Pb-Zn deposit of epithermal type in the eastern part of the Central Asian Orogenic Belt in NE China, to provide direct constraints on its metal source. Bulk ore samples and early-stage hydrothermal minerals (magnetite, pyrite, and quartz) show negative δ^{202}Hg (−1.52 to −0.18‰) and positive Δ^{199}Hg (−0.03 to 0.17‰) values similar to those of previously reported epithermal Au deposits in NE China, and also of marine systems in general. However, late-stage calcite shows weak negative to positive δ^{202}Hg (-0.61 to 0.90‰) and significant negative Δ^{199}Hg (−0.18 to −0.02‰), similar to the Late Paleozoic sandstone country rocks (δ^{202}Hg, −1.09 to 0.76‰; Δ^{199}Hg, −0.09 to 0.04‰). Hydrothermally altered gabbro and diorite show large variations in δ^{202}Hg (−1.83 to 0.50‰) and Δ^{199}Hg (−0.14 to 0.15‰) which overlap with those of the ore and country rocks, indicating a mixed source. The Δ^{199}Hg signature in the bulk ore and early-stage hydrothermal minerals likely derives from dehydration of the subducted oceanic slab, whereas Hg in late-stage calcite is likely derived from the sedimentary country rocks. Hydrothermal deposits in different tectonic settings have distinct Δ^{199}Hg signals, and our study suggests that Hg isotopes are a robust tool to distinguish metal sources of hydrothermal ore deposits.
© 2021 International Association for Gondwana Research. Published by Elsevier B.V. All rights reserved.

1. Introduction

The genesis of porphyry-epithermal deposits in volcanic-arc settings along subduction zones has attracted interest from economic geologists for decades due to their significant Cu, Mo, Au, Ag, Pb, and Zn resources (Sillitoe, 2010). While there is a consensus that arc magmatism plays an important role in the formation of porphyry-epithermal deposits (Hedenquist and Lowenstern, 1994; Sun et al., 2004; Cooke et al., 2005; Richards, 2009), the sources of the ore-forming components (including metals and their ligands) in the porphyry-epithermal ore deposit spectrum are still under debate. Economic geologists have attempted using traditional (e.g., S and Pb) and non-traditional isotopes (e.g., Tl, V, Fe, and Se) to trace the sources of the chalcophile elements in the igneous rocks and associated ore deposits (e.g., Prytulak et al., 2017; Williams et al., 2018; Kurzawa et al., 2019). However, the interplay of various processes from the roots of these systems, i.e. subduction-modified lithosphere, to the final mineral deposition site, i.e. the hydrothermal ore deposit, often blurs specific isotope signals. So far, ambiguities in the metal sources of these magmatic-hydrothermal deposits make it difficult to constrain their genesis and reconstruct their genetic models.

In low-temperature hydrothermal systems, mercury (Hg) shows a close association with Au, Ag, Sb, As, Pb, and Zn mineralization, due to its chalcophile nature (Bingqiu et al., 1986). Mercury has seven natural stable isotopes (^{196}Hg, ^{198}Hg, ^{199}Hg, ^{200}Hg, ^{201}Hg, ^{202}Hg, and ^{204}Hg), and is the only metal that undergoes both mass-dependent fractionation (usually defined as δ^{202}Hg) and mass-independent fractionation (MIF, usually defined as Δ^{199}Hg). Combined δ^{202}Hg and Δ^{199}Hg signals can be a powerful tracer as they provide multidimensional information on the sources and

* Corresponding author.
E-mail address: yinrunsheng@mail.gyig.ac.cn (R. Yin).

https://doi.org/10.1016/j.gr.2021.03.010
1751-7311/© 2021 International Association for Gondwana Research. Published by Elsevier B.V. All rights reserved.

processes of Hg in the environment (reviewed by Blum et al. (2014)). Since Smith et al. (2005) reported significant MDF of Hg isotopes in hydrothermal systems (δ^{202}Hg > 5‰), economic geologists have paid increasing attention to the use of Hg isotopes in revealing metal sources and hydrothermal processes in hydrothermal deposits (Smith et al., 2008; Sherman et al., 2009; Xu et al., 2018; Yin et al., 2019; Fu et al., 2020). Previous studies have shown that δ^{202}Hg can help to identify specific mineralization processes (e.g., boiling, redox reactions, and mineral precipitation) in a hydrothermal system (Smith et al., 2005; 2008; Sherman et al., 2009; Tang et al., 2017). Some studies observed large variations of Δ^{199}Hg in hydrothermal deposits (-0.30 to 0.36‰) as well (Deng et al., 2021 and references therein). Hg-MIF mainly occurs during photochemical processes, e.g., Hg(II) photoreduction and methylmercury (MeHg) photodegradation on Earth's surface (Bergquist and Blum, 2007). Hg-MIF signals observed in hydrothermal deposits have been explained by the contribution of Hg from surface Hg pools such as terrestrial and oceanic reservoirs (e.g., Deng et al., 2021). Therefore, Δ^{199}Hg can be used to trace the sources of ore-forming metals in hydrothermal systems, and is a sensitive monitor of the involvement of surface environments.

To better understand the Hg isotope geochemistry in epithermal deposits along convergent plate margins, we conducted a case study on the recently discovered large Erdaokon epithermal Ag-Pb-Zn deposit in the Duobaoshan Au-Cu polymetallic belt, NE China. We investigated the concentration and isotopic composition of Hg in bulk ore, hydrothermal minerals (including early-stage magnetite, pyrite, and quartz, and late-stage calcite), wall rocks, as well as the regionally distributed country rocks, and validated Hg isotopes as an effective tracer of (1) metal sources in hydrothermal deposits, and (2) metal recycling in subduction zones.

2. Geological setting

2.1. Regional geology

The Duobaoshan Au-Cu polymetallic belt, where the Erdaokan Ag-Pb-Zn deposit and many porphyry Cu-Mo deposits, epithermal

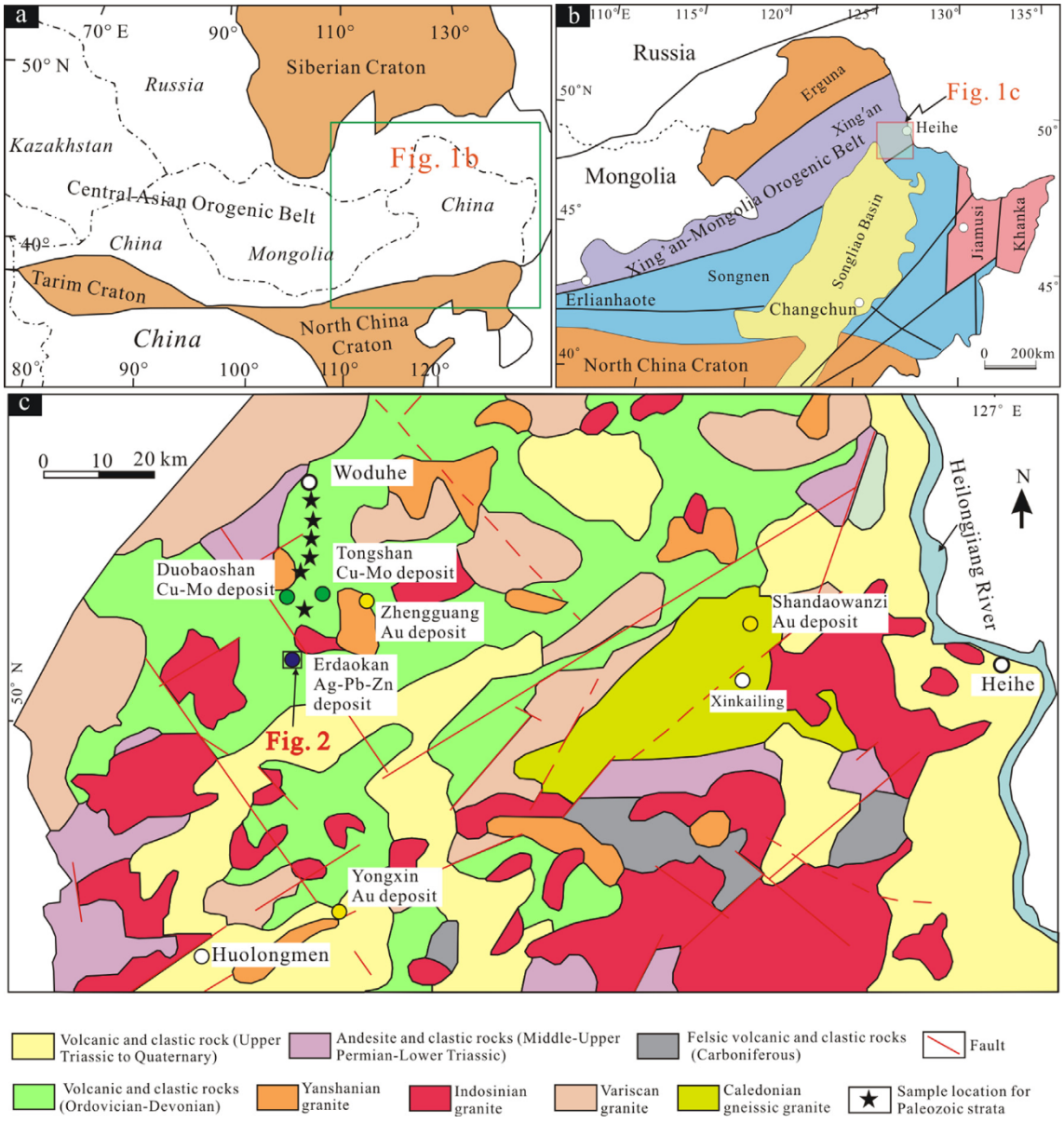

Fig. 1. (a) Tectonic sketch map of the Central Asian Orogenic Belt (after Jahn, 2004). (b) Tectonic map of NE China, showing the location of the studied area (modified after Xu et al., 2014). (c) Simplified geological map of the Nenjiang-Heihe area, showing the location of the Erdaokan Ag-Pb-Zn deposit (modified after Wu et al., 2015; Yuan et al., 2019).

Au deposits, and skarn type Pb-Zn deposits are located (Han et al., 2004; Cai et al., 2021; Yuan, 2020), is one of the most important metallogenic belts in NE China. The Duobaoshan polymetallic belt is situated in the eastern Central Asian Orogenic Belt (CAOB), which is located between the Siberia and North China cratons (Fig. 1a), and characterized by the multistage subduction of paleo-oceanic plates, and the amalgamation of several terranes (Erguna, Xing'an, Songnen, Jiamusi-Khanka blocks) (Fig. 1b). The Paleozoic tectonic evolution of the Duobaoshan polymetallic belt along the southeastern margin of the Xing'an Block is dominated by the Paleo-Asian Ocean tectonic regime. In the Early Paleozoic, the closure of a branch of the Paleo-Asian Ocean between the Erguna and Xing'an blocks caused the amalgamation of these two blocks (Ge et al., 2007). During the Ordovician-Early Carboniferous, the Duobaoshan polymetallic belt was in an active continental margin setting due to the northwestward subduction of the Paleo-Asian oceanic slab between the Xing'an and Songnen blocks (Deng et al., 2018). In the Late Paleozoic-Early Mesozoic, the Duobaoshan area came into a post-collision extensional setting after the closure of the Paleo-Asian Ocean in the Early Carboniferous (Xu et al., 2020). From the Triassic to the Early Jurassic, the tectonic evolution of the Duobaoshan area and its adjacent terrane is dominated by the southward subduction of the Mongol-Okhotsk oceanic slab (Zhao et al., 2019). In the Late-Jurassic-Early Cretaceous, magmatism and tectonic evolution in the Duobaoshan area were controlled by the westward subduction of the Paleo-Pacific oceanic slab (Xu et al., 2020). Complex tectonic processes lead to the formation of a series of NW-SE and NNE-SSW trending strike-slip and normal faults (Hao et al., 2015). The ore bodies in the Duobaoshan and Tongshan Cu-Mo deposits, Erdaokan Ag-Pb-Zn deposit, and Zhengguang and Yongxin Au deposits are all controlled by NW-SE trending structures (Han et al., 2004; Yuan et al., 2019).

Country rocks are the Early Paleozoic clastic-volcanic rocks, and Mesozoic volcanic rocks with minor Late Paleozoic-Early Mesozoic clastic rocks (Fig. 1c). The early Paleozoic strata consist mainly of the Early Ordovician Duobaoshan and Tongshan formations comprising andesite, dacite, and felsic volcani clastic rocks, the Early Silurian Huanghuagou, Woduhe, and Early Silurian-Middle Devonian Niqiuhe formations comprising terrestrial sandstone, siltstone, slate with minor limestone and volcanic rocks. The Late Mesozoic strata consist mainly of the Early Cretaceous Jiufengshan, Longjiang and Guanghua formations. The Jiufengshan Formation is a fan-delta sedimentary system of coarse debris gravity flow deposits (glutenite). The Longjiang and Guanghua formation consist mainly of andesite and rhyolite, respectively. Intrusive magmatism in the Duobaoshan polymetallic belt is relared to the Caledonian, Variscan, Indosinian, and Yanshannian periods (Zhao and Zhang, 1997; Wu et al., 2015). The intrusive rocks are composed of Cambrian gneissic granite, Ordovician monzodiorite, Carboniferous-Permian A-type granite and granodiorite, Jurassic granodiorite and monzonite, and Early Cretaceous alkali feldspar granite, diorite and adakitic granodiorite porphyry (Xu et al., 2020 and reference therein).

2.2. Deposit geology

The Erdaokan Ag-Pb-Zn deposit is located 125 km west of Heihe city, Heilongjiang Province, NE China. It contains proven reserves of 1000 t Ag with an average grade of 380 g/t Ag (Yuan et al., 2019). The lithostratigraphic units in the Erdaokan ore field are mainly Silurian-Devonian and Early Cretaceous (Fig. 2). The Silurian-Devonian strata consist of the Niqiuhe Formation comprising terrestrial siltstone and sandstone. The Cretaceous strata include the Longjiang and Guanghua formations consisting of andesite in the former and rhyolite in the latter. Intrusive rocks in the ore field are composed of Triassic gabbro and diorite (with zircon U-Pb ages of 226–234 Ma; Xu et al., 2019), and Early Cretaceous granite. There are two major ore bodies (Ore-body I and Ore-body II) and eight small ones, occurring as brecciated pinch-and swell veins along a NW-trending fault, dipping steeply SW (Fig. 2). The ore bodies are mainly hosted in the reddish-grey sandstone of the Upper Silurian to Middle Devonian Niqiuhe Formation (Fig. 2) and are commonly in contact with gabbro and diorite at depth (Yuan, 2020). Sandstone, gabbro, and diorite adjacent to ore bodies are strongly affected by hydrothermal alteration, expressed by carbonatization, silicification, kaolinization, sericitization, and pyritization.

The ore minerals consist mainly of pyrite, magnetite, hematite, galena, sphalerite, tetrahedrite, pyrargyrite, argentite, and marcasite. The gangue minerals are composed mainly of quartz, K-feldspar, calcite, gypsum, bitumen, and muscovite. A detailed description of ore structure and mineralogy is in Yuan et al. (2019). Based on the hydrothermal mineral associations and cross-cutting relationships, the hypogene mineralization is divided into three stages: magnetite-K-feldspar-quartz-hematite stage (I),

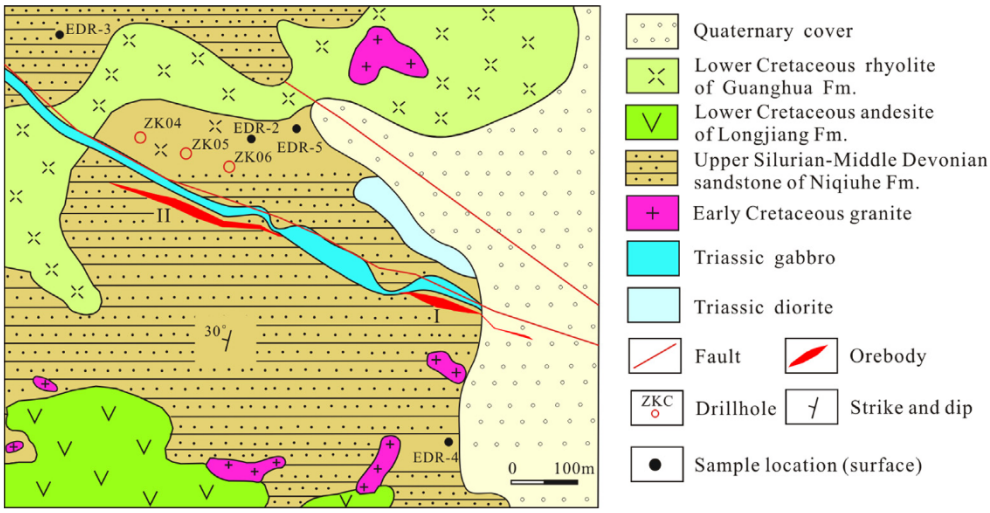

Fig. 2. Geological map of the Erdaokan Ag-Pb-Zn deposit (modified after Yuan et al., 2019).

silver-sulfide-quartz stage (II), and quartz-calcite stage (III). Stage I is characterized by massive and banded magnetite, K-feldspar, colorless quartz, and hematite occurring in the brecciated ores (Fig. 3-a-c) and cut by late-stage quartz and pyrite veins (Fig. 3d). Stage II is distinguished by smoky-grey quartz and abundant sulfide minerals such as pyrite (Fig. 3d-e), galena (Fig. 3f), sphalerite (Fig. 3g), tetrahedrite, pyrargyrite (Fig. 3h-i), and argentite (Fig. 3j). This stage is the main silver mineralization stage. Stage III is characterized by white quartz-calcite and pure calcite veins and veinlets occurring mainly within the wall rocks and minor in ore bodies (Fig. 3k-l). The age of the Erdaokan deposit is constrained by a Rb-Sr date on sulfides with 233 Ma (Yuan, 2020), similar to the neighboring Zhengguang epithermal Au system and the Tongshan Cu-Mo porphyry system (Cai et al., 2021). Fluid inclusion study shows that the ore-forming fluids were characterized by low salinity (0.35–5.54 wt% NaCl equivalent) and low density (0.89–1.1 g/cm^3), and the Ag-bearing minerals were precipitated at low temperatures (79-191℃) (Yuan et al., 2019). The mineral assemblage suggests an affiliation to the distal adularia-sericite type of epithermal systems (Heald et al., 1987) where the volcanic superstructure has been eroded.

3. Samples and analytical methods

Sixty-six samples from the Erdaokan Ag-Pb-Zn deposit were collected from drill core of three drill holes (ZK04, ZK05, and ZK06; Fig. 2). The samples include bulk ore (12), and wall rock: sandstone of the Niqiuhe Formation (10), gabbro (8), and diorite (6). Magnetite (n = 6, stage I), pyrite (n = 6, stage II), and quartz (n = 8, stage II) samples were handpicked from the ore samples. Calcite samples (n = 10, stage III) were handpicked from calcite veinlets in sandstone and altered gabbro. In addition, 15 rock samples from the Paleozoic strata outside of the Erdaokan deposit were also collected for comparison (Sample locations see Fig. 1c). Details of the samples are given in Supplementary **Table 1**. The samples were cleaned, dried, powdered to 200 mesh size and homogenized, before chemical analysis.

Total Hg (THg) concentrations of the samples were measured at the Institute of Geochemistry, Chinese Academy of Sciences using a DMA-80 Hg analyzer. Measurements of standard reference material (GSS-4, soil) showed recoveries of 90–110%. Coefficients of variation for triplicate analyses were < 10%.

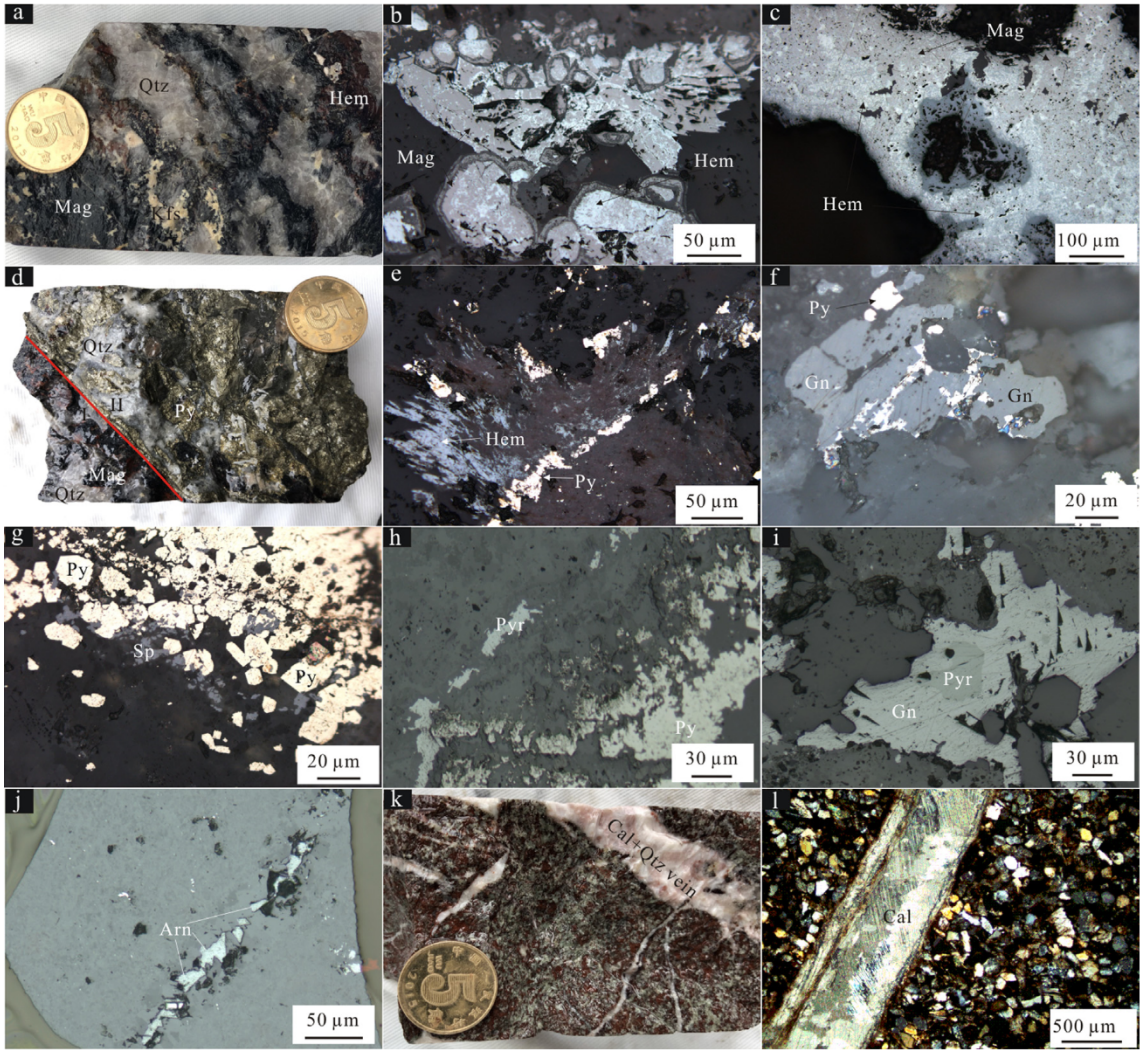

Fig. 3. (a-c) Ore samples with early-stage (I) mineral associations of quartz + magnetite + hematite + K-feldspar. (d) Pyrite + quartz vein (Stage II) crosscutting the magnetite + quartz veinlet (Stage I). (e) Stage II pyrite crosscutting the Stage I hematite and magnetite. (f) Galena and pyrite occurring together. (g) Pyrite and sphalerite occurring together in quartz vein. (h-i) Relationships of pyrargyrite, pyrite and galena. (j) Argentite in quartz vein. (k-l) Stage III calcite and quartz veinlets in wall rocks. Hem-hematite; Mag-Magnetite; Qtz-quartz; Py-pyrite; Gn-galena; Cal-calcite; Arn-Argentite; Pyr-pyrargyrite, Sp-sphalerite.

The samples were prepared for Hg isotope analysis following the double-stage thermal combustion and pre-concentration protocol (see detailed method in Zerkle et al. (2020). Standard reference material (GSS-4, soil) was prepared in the same way as the samples, which yielded Hg recoveries of 90–100%. The preconcentrated solutions were diluted to 1 ng/mL Hg and measured by a Neptune Plus multi-collector inductively coupled plasma mass spectrometer (MC-ICP-MS) at the Institute of Geochemistry, Chinese Academy of Sciences, following the method by Yin et al. (2016). Hg-MDF is expressed in δ^{202}Hg notation in units of ‰ referenced to the NIST-3133 Hg standard (analyzed before and after each sample):

$\delta^{202}Hg(‰) = [(^{202}Hg/^{198}Hg_{sample})/(^{202}Hg/^{198}Hg_{standard}) - 1] \times 1000$

MIF is reported in Δ notation, which describes the difference between the measured δ^{xxx}Hg and the theoretically predicted δ^{xxx}-Hg value, in units of ‰:

$\Delta^{xxx}Hg = \delta^{xxx}Hg - \delta^{202}Hg \times \beta$

β is 0.2520 for ^{199}Hg, 0.5024 for ^{200}Hg, and 0.7520 for ^{201}Hg (Blum and Bergquist, 2007).

Analytical uncertainty was estimated based on the replication of the NIST-3177 standard solution. The overall average and uncertainty of NIST-3177 (δ^{202}Hg: −0.50 ± 0.10‰; Δ^{199}Hg: −0.01 ± 0.06‰; Δ^{201}Hg: −0.02 ± 0.07‰, 2SD, n = 15) and GSS-4 (δ^{202}Hg: −1.67 ± 0.14‰; Δ^{199}Hg: −0.36 ± 0.07‰; Δ^{201}Hg: −0.38 ± 0.06‰, 2SD, n = 4) agrees well with previous studies (Blum and Bergquist, 2007; Sun et al., 2019). The 2SD of NIST-3177 with δ^{202}Hg, Δ^{199}Hg,and Δ^{201}Hg of respectively 0.10, 0.06 and 0.07 represent the analytical uncertainties of our samples.

4. Results

4.1. Hg concentrations

Hg concentration varies largely among the studied samples (Supplementary **Table S1**). The highest Hg concentrations are observed in pyrite (8.17–20.7 ppm) and bulk ore samples (0.475–20.4 ppm), suggesting that Hg is an integral component of the ore system. No native Hg and Hg minerals (e.g., cinnabar) have been observed. The elevated Hg concentration in pyrite and ore samples implies that Hg may be largely present as isomorphic substitution (e.g., Fe(II) → Hg(II)) in sulfide minerals. The Hg component in the quartz samples could be largely from fluid inclusions. Intermediate Hg concentrations are observed in magnetite (0.047–0.772 ppm), altered gabbro (0.002–1.32 ppm), diorite (0.084–1.28 ppm), and sandstone (0.006–0.80 ppm). The lowest Hg concentrations are observed in fresh gabbro (0.024–0.049 ppm), quartz (0.008–0.091 ppm). The samples from the Paleozoic strata outside of the ore deposit can be considered as the regional reference system unaffected by hydrothermal overprint (0.002–0.026 ppm, with a mean of 0.010 ± 0.008 ppm Hg; n = 11).

4.2. Hg isotopic composition

The Hg isotopic composition of the studied samples is summarized in Supplementary **Table S1** and shown in Figs. 4-5. The overall variations of δ^{202}Hg (2.73‰) and Δ^{199}Hg (0.35‰) for all samples are 27 and 7 times of the analytical uncertainty (0.10‰ and 0.05‰ for δ^{202}Hg and Δ^{199}Hg, respectively). Specifically, the bulk ore samples show δ^{202}Hg of −1.52 to −0.66‰ and Δ^{199}Hg of −0.03 to 0.16‰; The sandstone samples from the Niqiuhe Formation show higher δ^{202}Hg of −1.09 to 0.76‰ and lower Δ^{199}Hg of −0.09 to 0.04‰; The altered gabbro and diorite samples show large variations of δ^{202}Hg (-1.52 to 0.45‰, and-1.83 to 0.50‰, respectively) and Δ^{199}Hg (-0.14 to 0.15‰, and −0.04 to 0.08‰, respectively). The rock samples from far outside the ore deposit show δ^{202}Hg (-1.62 to 0.09‰) and Δ^{199}Hg (-0.08 to 0.01‰) values similar to those of the wall rocks of the ore bodies.

The hydrothermal pyrite samples show a narrow range of δ^{202}Hg (-1.16 to −0.86‰) and Δ^{199}Hg (0.06 to 0.15‰). Magnetite and quartz samples show δ^{202}Hg (-1.42 to −0.18‰, and −1.14 to −0.43‰, respectively) and Δ^{199}Hg (0.05 to 0.17‰, and 0.01 to

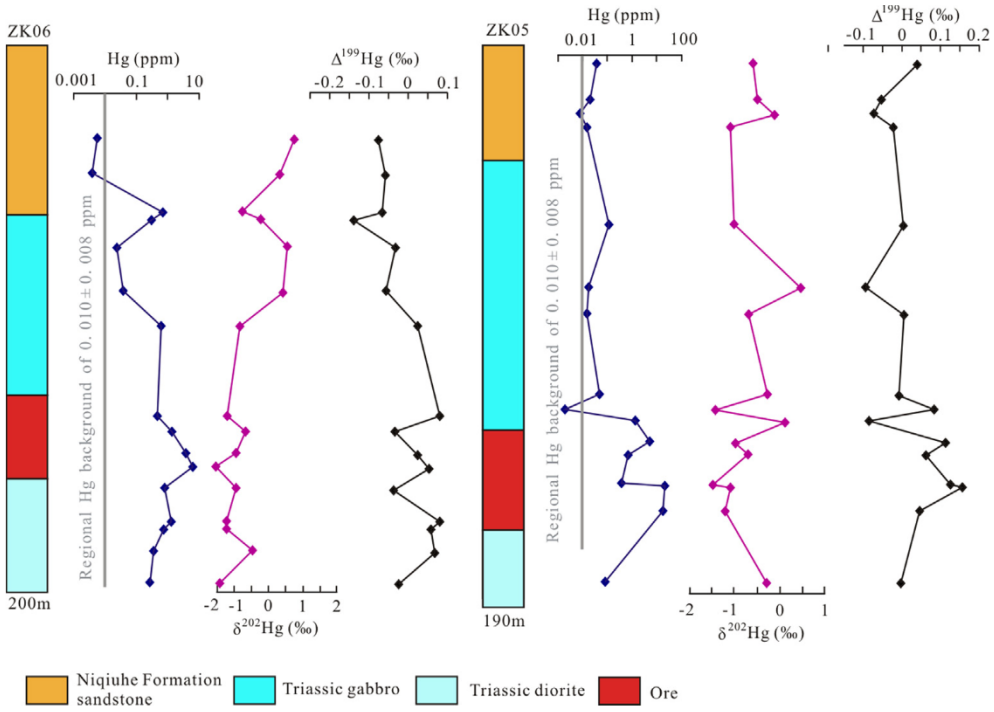

Fig. 4. Vertical profiles showing the distribution of Hg concentrations and isotopic compositions in drill holes No. ZK06 and ZK05 from the Erdaokan Ag-Pb-Zn deposit. Data and sample numbers in Supplementary Table 1.

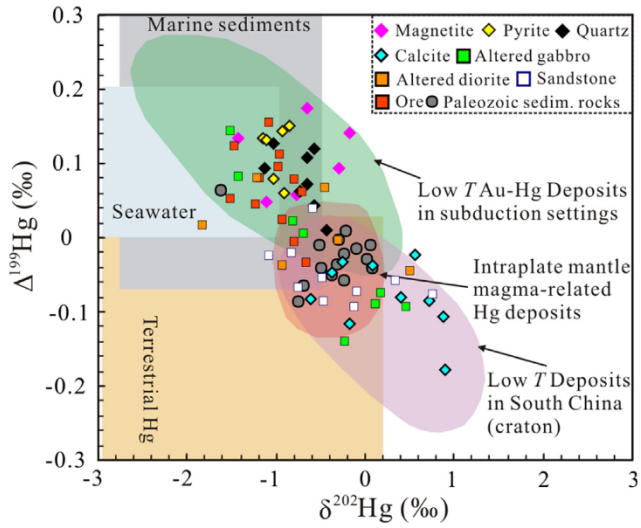

Fig. 5. Δ^{199}Hg versus δ^{202}Hg diagram for the samples studied. Reference fields for gold deposits in NE China, Hg deposits worldwide, and Au-Sb-Pb-Zn deposits in South China see Deng et al. (2021) and reference therein. Area of terrestrial Hg is defined by Blum et al. (2014, and references therein), marine sediments is that defined by Yin et al. (2015) and Meng et al. (2019), and seawater is that defined by Štrok et al. (2015).

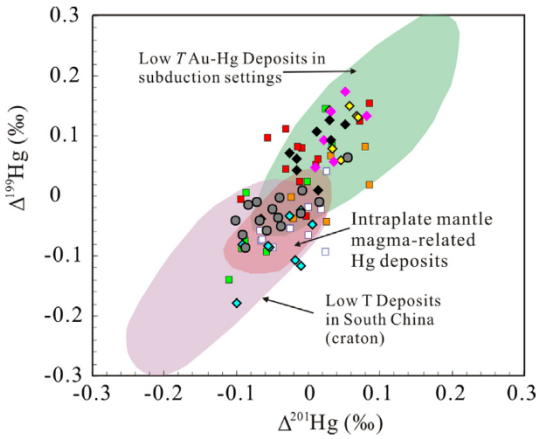

Fig. 6. Δ^{199}Hg versus Δ^{201}Hg diagram for the samples studied. Reference fields for gold deposits in NE China, Hg deposits worldwide, and Au-Sb-Pb-Zn deposits in South China from Deng et al. (2021).

0.13‰, respectively), values similar to pyrite. The calcite samples show higher δ^{202}Hg (-0.61 to 0.90‰) and lower Δ^{199}Hg (-0.18 to −0.02‰) than the early stage pyrite, magnetite, and quartz samples.

5. Discussion

5.1. Hg isotopes reflect Hg from two sources

The bulk ore and hydrothermal minerals from stage I and II (magnetite, pyrite, and quartz) in the Erdaokan deposit are characterized by negative δ^{202}Hg values, which are within the range reported for ore samples of Hg deposits worldwide (Fig. 5), but different from that observed in mantle materials (δ^{202}Hg of ~ 0‰, Sherman et al., 2009). The late-stage calcite samples show weak negative to significant positive δ^{202}Hg values (Fig. 5), which are different from the early-stage minerals. Previous studies have inferred that significant Hg-MDF is probably triggered by boiling of hydrothermal fluids, redox reactions, and mineral precipitation (Smith et al., 2005; 2008; Sherman et al., 2009; Tang et al., 2017). In this study, although the redox conditions of the ore-forming fluid changed from stage I (magnetite: oxidized) to Stage II (pyrite: reduced), no significant differences in δ^{202}Hg are observed in magnetite and pyrite (Fig. 5), precluding redox reactions as a dominant factor triggering the Hg-MDF. These minerals formed under similar pressure conditions ruling out the dominant factor of boiling of the hydrothermal fluids, which was suggested causing distinct Hg-MDF at different depth levels of a hydrothermal system (Smith et al., 2005). Therefore, significant differences in δ^{202}Hg among hydrothermal minerals are likely caused by different mobilization processes of Hg, including released or leached Hg from different sources and final precipitation. Previous work showed that mobilization of Hg from source rocks causes a shift of δ^{202}Hg (<0.6‰) (Smith et al., 2008) and that lighter Hg isotopes are preferentially fixed in ore minerals (Sherman et al., 2009).

The observation of distinct Hg-MIF in our samples, with Δ^{199}Hg ranging from −0.18 to 0.17‰, is consistent with recent studies on Hg-MIF signals in hydrothermal Hg and Au deposits worldwide (Deng et al., 2021) (Fig. 5). As shown in Fig. 6, rock, bulk ore, and hydrothermal mineral samples in the Erdaokan deposit show a Δ^{199}Hg/Δ^{201}Hg ratio of ~ 1.0, suggesting aqueous Hg(II) photoreduction is the main driver for the formation of the observed Hg-MIF (Bergquist and Blum, 2007). Earth's surface Hg pools such as oceanic (e.g., marine sediments and seawater) and terrestrial reservoirs (e.g., soil and vegetation) are characterized by positive and negative Δ^{199}Hg signals (Fig. 5), respectively, and are different from mantle-derived Hg with Δ^{199}Hg ~ 0 (Sherman et al., 2009). Previous studies also suggested that Hg-MIF unlikely occurs during hydrothermal processes (Smith et al., 2008; Yin et al., 2016). Therefore, the observation of Hg-MIF in the Erdaokan deposit suggests a contribution of Hg from Earth's surface Hg pools - not dominantly from the mantle.

A negative correlation between δ^{202}Hg and Δ^{199}Hg can be observed in the Erdaokan deposit (Fig. 5), suggesting mixing of Hg from two sources. By looking at the data in detail, a significant positive correlation is observed for δ^{202}Hg vs. 1/Hg and a negative correlation for Δ^{199}Hg v.s 1/Hg (Fig. 7). Two Hg end-members can therefore be identified according to these correlations: a high-Hg end-member with lower δ^{202}Hg and positive Δ^{199}Hg (Source 1) which characterizes the ore, and a low-Hg end-member with δ^{202}Hg and lower Δ^{199}Hg (Source 2) which corresponds to the country rocks. The hydrothermally altered gabbro and diorite samples show a large variation in Hg isotopic composition overlapping with the two end-members (Figs. 6 and 7), indicating variable degree of mixing sources.

5.2. Contribution of metals from the oceanic slab and implications for the genesis of the Erdaokan Ag-Pb-Zn deposit

The absence of adakitic rocks in the Erdaokan deposit, which commonly show great affinity with porphyry-epithermal deposits (Thieblemont et al., 1997) and which were suggested to be derived from partial melting of thick lower continental crust or oceanic slab melting (e.g., Defant and Drummond, 1990; Kay and Mpodozis, 2001), preclude the contribution of Hg from thick continental crust or oceanic crustal melts. The Triassic diorite and gabbro in the studied deposit, which are contemporaneous with ore formation (Xu et al., 2019) and control the ore deposit (Fig. 2), indicate that the ore-forming metals are likely carried by mantle-derived magma. This is also suggested by the abundance of tellurium occurring as isomorphic substitution in the Ag-bearing sulfides in the Erdaokan deposit (Xu et al., 2019), which is considered diagnostic for magma or degasification of the mantle (Rubin,

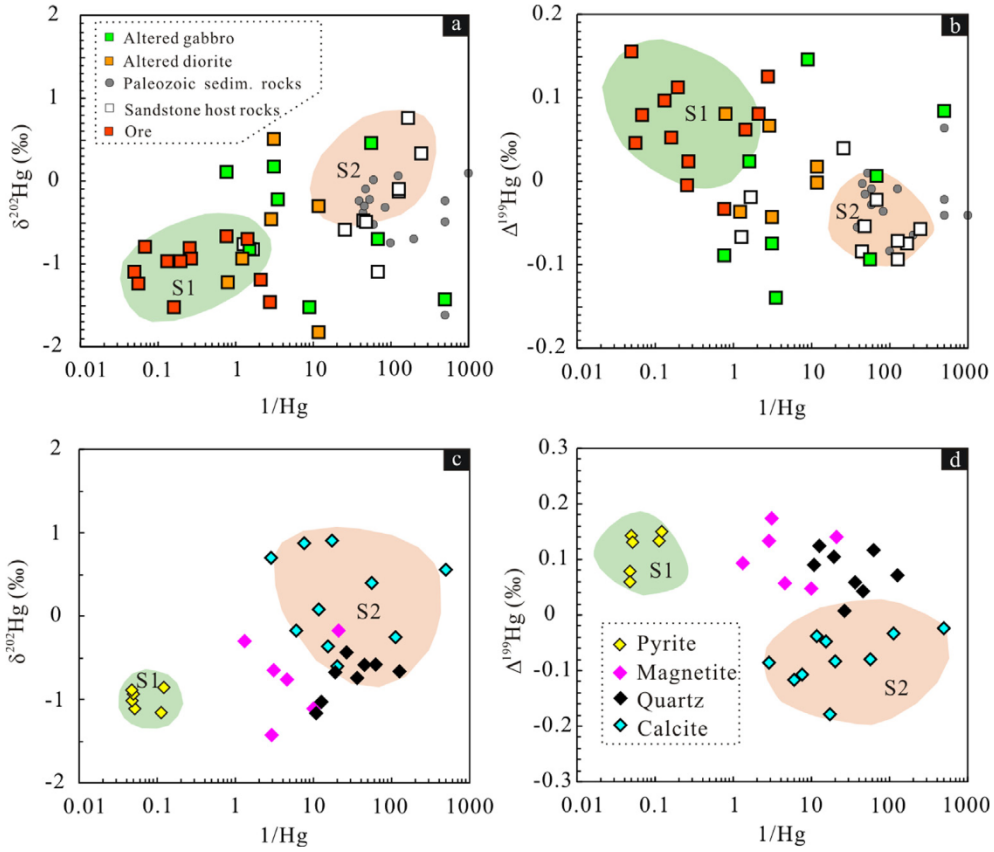

Fig. 7. Plots of δ^{202}Hg vs. 1/Hg and Δ^{199}Hg vs. 1/Hg of rock samples (a-b) and hydrothermal mineral samples (c-d) in the Erdaokan Ag-Pb-Zn deposit, showing two Hg sources in the Erdaokan hydrothermal system.

1997). However, the significant positive and marine-like Δ^{199}Hg values of the bulk ore, magnetite, pyrite, and quartz samples preclude a direct mantle source for Hg (Δ^{199}Hg ~ 0; Sherman et al., 2009). Given that the regionally distributed Paleozoic clastic rocks have negative Δ^{199}Hg values (Supplementary Table S1) and the lack of marine shales which commonly have positive Δ^{199}Hg values (Blum et al., 2014), we propose that the enrichment of Hg in the Erdaokan deposit was likely related to the subducted slab which carries the positive Δ^{199}Hg signature of seawater fixed in marine shale and altered oceanic crust.

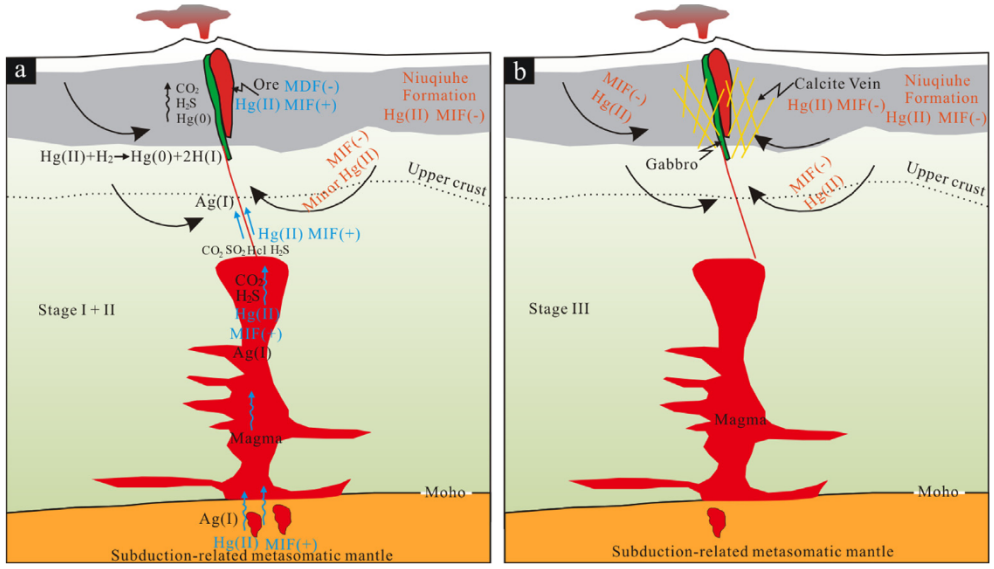

Fig. 8. Cartons showing the mineralization process and Hg isotopic geochemistry of the Erdaokan Ag-Pb-Zn deposit. (a) Contribution of magmatic fluids with elevated Hg concentration and with positive Δ^{199}Hg released from the subducting oceanic slab. This fluid characterizes the stage I and II of the ore system. (b) Contribution of meteoric water with low concentrations of Hg with negative Δ^{199}Hg leached from the sandstone country rock of the Niqiuhe Formation. This fluid characterizes the stage III of the ore system and propylitic alteration in the wall rocks.

The Erdaokan area has experienced an active continental margin setting dominated by the southward subduction of the Mongol-Okhotsk Ocean during the Triassic (Yuan et al., 2019). This is evident by the occurrence of Triassic subduction-related magmatic rocks derived from the metasomatized mantle wedge (Li et al., 2017), indicating the involvement of fluids derived from the downgoing oceanic slab. In the subduction zone, sulfides together with pelagic clays may be among the first phases to destabilize and contribute to slab-derived fluid signatures (Kurzawa et al., 2019). Hg and other chalcophile elements (e.g., Cu, Mo, Au, Ag, Pb, and Zn) are predominantly hosted by or absorbed onto sulfides (Bower et al., 2008). During the dehydration of the oceanic slab, Hg and other chalcophile elements may migrate from sediments and altered oceanic crust as proposed by Deng et al. (2021). These components can be transported in transcrustal magmatic systems, released into magmatic-hydrothermal fluids, and finally precipitated in shallow epithermal systems (Fig. 8a). The initially magmatic-hydrothermal fluids become gradually dominated by external meteoric water as expressed by the quartz-calcite stage, or propylitic alteration, whereby the sedimentary country rocks are leached (Fig. 8b). Therefore, Hg in the late calcite veins shows negative Δ^{199}Hg values similar to the sedimentary country rocks.

5.3. Implications for metal tracing in hydrothermal systems using Hg isotopes

On the example of the Erdaokan deposit, our study shows that the comparison of Hg isotopes between country rock and ore can help to identify Hg source endmembers. The distinct difference in Hg-MIF signals between early-stage and late-stage hydrothermal minerals reflects the shift from a magmatic-hydrothermal to a non-magmatic-hydrothermal fluid system (in our epithermal case: meteoric-hydrothermal). Taking into account the data of previous work on low-temperature vein-style deposits in South China (Fig. 5), the different tectonic settings of the subduction-related epithermal system and the intracontinental hydrothermal ore systems in South China become apparent. The latter systems can be related to metamorphic fluids which have no marine signature (Deng et al., 2021).

6. Conclusions

The systematic study of the isotopic composition of Hg in bulk ore and hydrothermal minerals in the Erdaokan Ag-Pb-Zn deposit and its Paleozoic country rocks allows the following conclusions:

(1) The distinct change in Hg isotopic characteristics from the early and main stage mineralization to the late stage indicates that the metal source varies during the evolution of the hydrothermal system.
(2) Positive Hg-MIF signals identify a significant metal contribution from the subducted oceanic slab and reflect the subduction setting of the ore system.
(3) The compilation of Hg isotopic data from hydrothermal ore deposits worldwide indicates distinct Δ^{199}Hg signals in hydrothermal deposits of different tectonic settings.
(4) We conclude that Hg isotopes can be used as a new tracer for the source of metals in hydrothermal ore deposits and their geotectonic setting.

CRediT authorship contribution statement

Changzhou Deng: Conceptualization, Resources, Methodology, Software, Writing - original draft. **Chenglu Li:** Resources, Investigation. **Yimeng Rong:** Investigation, Formal analysis. **Di Chen:** Investigation, Formal analysis. **Ting Zhou:** Investigation, Formal analysis. **Xueyun Wang:** Investigation, Formal analysis. **Huayong Chen:** Conceptualization, Writing - review & editing. **Bernd Lehmann:** Conceptualization, Writing - review & editing. **Runsheng Yin:** Methodology, Funding acquisition, Writing - review & editing.

Declaration of Competing Interest

The authors declare that they have no known competing financial interests or personal relationships that could have appeared to influence the work reported in this paper.

Acknowledgments

This work was supported by the National Natural Science Foundation of China (grants 41873047, 41603020 and 41872038). We especially thank Jishuang Ding for help with field sampling, and Editor Franco Pirajno, Meifu Zhou and anonymous Reviewer for their useful comments.

Appendix A. Supplementary data

Supplementary data to this article can be found online at https://doi.org/10.1016/j.gr.2021.03.010.

References

Bergquist, B.A., Blum, J.D., 2007. Mass-dependent and -independent fractionation of Hg isotopes by photoreduction in aquatic systems. Science 318, 417–420.
Bingqiu, Z., Jinmao, Z., Lixin, Z., Yaxin, Z., 1986. Mercury, arsenic, antimony, bismuth and boron as geochemical indicators for geothermal areas. J. Geochem. Explor. 25, 379–388.
Blum, J.D., Bergquist, B.A., 2007. Reporting of variations in the natural isotopic composition of mercury. Anal. Bioanal. Chem. 388, 353–359.
Blum, J.D., Sherman, L.S., Johnson, M.W., 2014. Mercury isotopes in earth and environmental sciences. Annu. Rev. Earth Planet. Sci. 42, 249–269.
Bower, J., Savage, K.S., Weinman, B., Barnett, M.O., Hamilton, W.P., Harper, W.F., 2008. Immobilization of mercury by pyrite (FeS_2). Environ. Pollut. 156, 504–514.
Cai, W.Y., Wang, K.Y., Li, J., Fu, L.J., Lai, C.K., Liu, H.L., 2021. Geology, geochronology and geochemistry of large Duobaoshan Cu-Mo-Au orefield in NE China: Magma genesis and regional tectonic implications. Geosci. Front. 12, 265–292.
Cooke, D.R., Hollings, P., Walshe, J.L., 2005. Giant porphyry deposits: Characteristics, distribution, and tectonic controls. Econ. Geol. 100, 801–818.
Defant, M.J., Drummond, M.S., 1990. Derivation of some modern arc magmas by melting of young subducted lithosphere. Nature 347, 662–665.
Deng, C.Z., Sun, G.Y., Rong, Y.M., Sun, R.Y., Sun, D.Y., Lehmann, B., Yin, R.s., 2021. Recycling of mercury from the atmosphere-ocean system into volcanic-arc-associated epithermal gold systems. Geology 49, 309-313.
Deng, C.Z., Sun, D.Y., Sun, G.Y., Lv, C.L., Qin, Z., Ping, X.Q., Li, G.H., 2018. Age and geochemistry of Early Ordovician A-type granites in the northeastern Songnen Block. NE China. Acta Geochim. 37, 805–819.
Ge, W.C., Sui, Z.M., Wu, F.Y., Zhang, J.H., Xu, X.C., Cheng, R.Y., 2007. Zircon U-Pb ages, Hf isotopic characteristics, and their implications of the Early Paleozoic granites in the northeastern Da Hinggan Mountains, northeastern China. Acta Petrol. Sin. 23, 423–440 (in Chinese with English abstract).
Fu, S.L., Hu, R.Z., Yin, R.S., Yan, J., Mi, X.F., Song, Z.C., Sullivan, N.A., 2020. Mercury and in situ sulfur isotopes as constraints on the metal and sulfur sources for the world's largest Sb deposit at Xikuangshan. Southern China. Mineral. Deposita 55, 1353–1364.
Han, Z.X., Xu, Y.Q., Zheng, Q.D., 2004. Metallogenetic series and evolution of signifificant metal and nonmetal mineral resources in Heilongjiang province. Heilongjiang People's Publishing. In: House, Harbin (Ed.), (in Chinese with. English abstract).
Hao, Y.J., Ren, Y.S., Duan, M.X., Tong, K.Y., Chen, C., Yang, Q., Li, Ch., 2015. Metallogenic events and tectonic setting of the Duobaoshan ore field in Heilongjiang Province. NE China. J. Asian Earth Sci. 97, 442–458.
Heald, P., Foley, N.K., Hayba, D.O., 1987. Comparative anatomy of volcanic-hosted epithermal deposits: Acid-sulfate and adularia-sericite type. Econ. Geol. 82, 1–26.
Hedenquist, J.W., Lowenstern, J.B., 1994. The role of magmas in the formation of hydrothermal ore deposits. Nature 370, 519–527.
Jahn, B.M., 2004. The Central Asian Orogenic Belt and growth of the continental crust in the Phanerozoic. Geol. Soc. London, Special Publ. 226, 73–100.
Kay, S.M., Mpodozis, C., 2001. Central Andean ore deposits linker to evolving shallow subduction systems and thickening crust. GCA Today, 4–9.

Kurzawa, T., Konig, S., Alt, J.C., Yierpan, A., Schoenberg, R., 2019. The role of subduction recycling on the selenium isotope signature of the mantle: Constraints from Mariana arc lavas. Chem. Geol. 513, 239–249.
Li, Y., Xu, W.L., Wang, F., Pei, F.P., Tang, J., Zhao, S., 2017. Triassic volcanism along the eastern margin of the Xing'an Massif, NE China: Constraints on the spatial-temporal extent of the Mongol-Okhotsk tectonic regime. Gondwana Res. 48, 205–223.
Meng, M., Sun, R.Y., Liu, H.W., Yu, B., Yin, Y.G., Hu, L.G., Shi, J.B., Jiang, G.B., 2019. An integrated model for input and migration of mercury in Chinese coastal sediments. Environ. Sci. Technol. 53, 2460–2471.
Prytulak, J., Sossi, P.A., Halliday, A.N., Plank, T., Savage, P.S., Woodhead, J.D., 2017. Stable vanadium isotopes as a redox proxy in magmatic systems?. Geochem. Perspect. Lett. 3, 75–84.
Richards, J.P., 2009. Postsubduction porphyry Cu-Au and epithermal Au deposits: Products of remelting of subduction-modified lithosphere. Geology 37, 247–250.
Rubin, K., 1997. Degassing of metals and metalloids from erupting seamount and mid-ocean ridge volcanoes: observations and predictions. Geochim. Cosmochim. Ac. 61, 3525–3542.
Sherman, L.S., Blum, J.D., Nordstrom, D.K., McCleskey, R.B., Barkay, T., Vetriani, C., 2009. Mercury isotopic composition of hydrothermal systems in the Yellowstone Plateau volcanic field and Guaymas Basin sea-floor rift. Earth Planet. Sci. Lett. 279, 86–96.
Sillitoe, R.H., 2010. Porphyry copper systems. Econ. Geol. 105, 3–41.
Smith, C.N., Kesler, S.E., Klaue, B., Blum, J.D., 2005. Mercury isotope fractionation in fossil hydrothermal systems. Geology 33, 825–828.
Smith, C.N., Kesler, S.E., Blum, J.D., Rytuba, J.J., 2008. Isotope geochemistry of mercury in source rocks, mineral deposits and spring deposits of the California Coast Ranges, USA. Earth Planet. Sci. Lett. 269, 399–407.
Štrok, M., Baya, P.A., Hintelmann, H., 2015. The mercury isotope composition of Arctic coastal seawater: CR. Geosci. 347, 368–376.
Sun, R.Y., Jiskra, M., Amos, H.M., Zhang, Y.X., Sunderland, E.M., Sonke, J.E., 2019. Modeling the mercury stable isotope distribution of Earth surface reservoirs: Implications for global Hg cycling. Geochim. Cosmochim. Ac. 246, 156–173.
Sun, W.D., Richard, J.A., Vadim, S.K., Raymond, A.B., 2004. Release of gold-bearing fluids in convergent margin magmas prompted by magnetite crystallization. Nature 431, 975–978.
Tang, Y.Y., Bi, X.W., Yin, R.S., Feng, X.B., Hu, R.Z., 2017. Concentrations and isotopic variability of mercury in sulfide minerals from the Jinding Zn-Pb deposit. Southwest China. Ore Geol. Rev. 90, 958–969.
Thieblemont, D., Stein, G., Lescuyer, J.L., 1997. Gisements epithermaux et porphyriques: Ia connexion adakite. Earth Planet. Sci. Lett. 325, 103–109.
Williams, H.M., Prytulak, J., Woodhead, J.D., Kelley, K.A., Brounce, M., Plank, T., 2018. Interplay of crystal fractionation, sulfide saturation and oxygen fugacity on the iron isotope composition of arc lavas: an example from the Marianas. Geochim. Cosmochim. Ac. 226, 224–243.
Wu, G., Chen, Y., Sun, F., Liu, J., Wang, G.R., Xu, B., 2015. Geochronology, geochemistry, and Sr–Nd–Hf isotopes of the early Paleozoic igneous rocks in the Duobaoshan area, NE China, and their geological significance. J. Asian Earth Sci. 97, 229–250.
Xu, B., Zhao, P., Bao, Q.Z., Zhou, Y.H., Wang, Y.Y., Luo, Z.W., 2014. Preliminary study on the Pre-Mesozoic tectonic unit division of the Xing-Meng Orogenic Belt (XMOB). Acta Petrol. Sin. 30, 1841–1857 (in Chinese with English abstract).
Xu, C.X., Yin, R.S., Peng, J.T., Hurley, J.P., Lepak, R.F., Gao, J.F., Feng, X.B., Hu, R.Z., Bi, X. W., 2018. Mercury isotope constraints on the source for sediment-hosted lead-zinc deposits in the Changdu area, southwestern China. Mineral. Deposita 53, 339–352.
Xu, G.Z., Deng, C.Z., Li, C.L., Lv, C.L., Yin, R.S., Ding, J.S., Yuan, M.W., Gou, J., 2020. Petrogenesis of Late Carboniferous A-type granites and Early Cretaceous adakites of the Songnen Block, NE China: Implications for the geodynamic evolution of the Paleo-Asian and Paleo-Pacific oceans. Lithos 366–367, 105575.
Xu, W.X., Li, C.L., Bao, X.B., Yuan, M.W., Deng, C.Z., Yang, Y.G., Xu, G.Z., 2019. Geological characteristics and genesis analysis of the first Triassic silver deposit discovered in Northeast of Da Hinggan Mountains. Miner. Resour. Geol 33, 435–441 (in Chinese with English abstract).
Yin, R.S., Feng, X.B., Chen, B., Zhang, J., Wang, W., Li, X., 2015. Identifying the sources and processes of mercury in subtropical estuarine and ocean sediments using Hg isotopic composition. Environ. Sci. Technol. 49, 1347–1355.
Yin, R.S., Krabbenhoft, D.P., Bergquist, B.A., Zheng, W., Lepak, R.F., Hurley, J.P., 2016. Effects of mercury and thallium concentrations on high precision determination of mercury isotopic composition by Neptune Plus multiple collector inductively coupled plasma mass spectrometry. J. Anal. Atom. Spectrom. 31, 2060–2068.
Yin, R.S., Deng, C.Z., Lehmann, B., Sun, G.Y., Lepak, R.F., Hurley, J.P., Zhao, C.H., Xu, G. W., Tan, Q.P., Xie, G.Z., Hu, R.Z., 2019. Magmatic-hydrothermal origin of mercury in Carlin-style and epithermal gold deposits in China: evidence from mercury stable isotopes. ACS Earth Space Chem. 3, 1631–11369.
Yuan, M.W., 2020. The contribution of the bitumen to the mineralization of the non-stratabound metal deposit: Ag-Pb-Zn deposits in the Great Xing'an Range PhD Thesis. China University of Geosciences, Beijing.
Yuan, M.W., Li, L., Li, S.R., Li, C.L., Santosh, M., Alam, M., Bao, X.B., 2019. Mineralogy, fluid inclusions and S-Pb-H-O isotopes of the Erdaokan Ag-Pb-Zn deposit, Duobaoshan Metallogenic Belt, NE China: Implications for ore genesis. Ore Geol. Rev. 113, 103074.
Zerkle, A.L., Yin, R.S., Chen, C.Y., Li, X.D., Izon, G.J., Grasby, S.E., 2020. Anomalous fractionation of mercury isotopes in the Late Archean atmosphere. Nat. Commun. 11, 1709.
Zhao, C., Qin, K.Z., Song, G.X., Li, G.M., 2019. Switch of geodynamic setting from the Paleo-Asian Ocean to the Mongol-Okhotsk Ocean: Evidence from granitoids in the Duobaoshan ore field, Heilongjiang Province, Northeast China. Lithos 336–337, 202–220.
Zhao, Y.M., Zhang, D.Q., 1997. Metallogeny and prospective evolution of copper polymetallic deposits in the Great Xing'an Range and its adjacent regions. Seisnological Press, Beijing, pp. 48–82 (in Chinese).